Enhancing Icing Detection and Characterization Using the New York State Mesonet

JUNHONG WANG,[a,b] JERALD BROTZGE,[a] JACOB SHULTIS,[c] AND NATHAN BAIN[a]

[a] *New York State Mesonet, University at Albany, State University of New York, Albany, New York*
[b] *Department of Atmospheric and Environmental Sciences, University at Albany, State University of New York, Albany, New York*
[c] *The Johns Hopkins University, Baltimore, Maryland*

(Manuscript received 29 December 2020, in final form 24 June 2021)

ABSTRACT: The accurate detection and monitoring of freezing rain and icing conditions at the surface is a notoriously challenging but important problem. This work attempts to enhance icing detection and characterization utilizing data from the New York State Mesonet (NYSM). NYSM is the first operational network measuring winds at 10 m from two independent sensors: propeller and sonic anemometers. During and after freezing rain events, large wind speed differences are frequently reported between the two anemometers because the propeller develops a coating of ice, thus either stopping or slowing its rotation. Such errors of propeller data provide a signal for identifying icing conditions. An automated method for identifying ''active freezing rain'' (AFR) and a continuation of ''frozen surface'' (FS) conditions is developed. Hourly maps of AFR and FS sites are generated using four criteria: 1) a wind speed difference (sonic − propeller) of $>1\,m\,s^{-1}$ or $0\,m\,s^{-1}$ propeller wind speed for at least a half hour, 2) a temperature threshold of −5° to 2°C for AFR and less than 2°C for FS, 3) insignificant hourly snow accumulation, and 4) with (without) significant hourly precipitation accumulation for AFR (FS). The AFR events detected by the automated method for last four winters (2017–21) show very good agreements in starting and ending times with that from the Automated Surface Observing System (ASOS) data. A case study of the ice storm during 14–16 April 2018 further demonstrates the validity of the methodology and highlights the benefit of NYSM profiler and camera data.

KEYWORDS: Freezing precipitation; Icing; Measurements

1. Introduction

Winter weather has a strong impact on the economy, infrastructure, and people's daily lives. Among the most damaging and disruptive winter weather phenomena are ice storms. These intense freezing rain/freezing drizzle events lead to extremely hazardous conditions, which can last up to days or weeks, causing large amounts of damage to property and infrastructure over their duration (Degelia et al. 2016). Utility, transportation, aviation, communication, and public safety can suffer severe disruptions with impacts ranging from traffic accidents to power outages to closure of air travel (e.g., Fikke et al. 2008; Call 2010). Atmospheric ice can easily accrete on infrastructures including bridges (e.g., Andre et al. 2018; Abdelaal et al. 2019), power lines (Savadjiev and Farzaneh 2004), telecommunication towers (Mulherin 1998), and wind turbines (Homola et al. 2006). Ice storms can also lead to adverse ecological and silvicultural impacts on forests (e.g., Irland 2000; Bragg et al. 2003; Millward and Kraft 2004).

Ice storms are most common in the northwestern, north-central, and northeastern United States, with the highest frequency observed across the Northeast (Changnon 2003; Cortinas et al. 2004; Kovacik and Kloesel 2014; Degelia et al. 2016). Kovacik and Kloesel (2014) show that changes in the Northeast ice storm frequency are largely influenced by changes in global air circulation, particularly via teleconnection patterns, such as the Atlantic multidecadal oscillation (AMO), North Atlantic Oscillation (NAO), and El Niño–Southern Oscillation (ENSO). The durations of freezing rain events over North America also vary spatially and are most commonly shorter than 1 h with an exponential decrease in frequency with increasing duration (Cortinas et al. 2004; McCray et al. 2019). However, the long-duration (≥6 h) events are more frequent in the northeastern United States and southeastern Canada compared with other regions because of their unique thermodynamic characteristics (McCray et al. 2019, 2020).

To better understand the frequency and spatial occurrence of ice storms in New York State (NYS), we analyzed all ''ice storm'' events recorded across NYS in the National Centers for Environmental Information (NCEI) storm database (NCEI 2019) for the period of 1997–2019. Ice storms in the database are defined as when ice accretion meets or exceeds locally/regionally defined warning criteria (typical value is 1/4 or 1/2 in. or more; 1 in. = 2.54 cm) (NWS 2016). If the freezing rain was mixed with other precipitation types, then a ''winter storm'' event would be reported in the storm database. These events were not included in this analysis. Between 1997 and 2019, a total 46 ice storms were recorded in NYS in the NCEI database and impacted a cumulative 257 counties with a total $102 million in damages (Fig. 1). They show coherent spatial structure with the highest frequency in the Eastern Plateau region (Fig. 1). This is due to the complex terrain that assists in creating freezing rain conditions and the high frequency of frontal systems in the region during the winter months. Note that the spatial distribution of total damage is not consistent with that of the frequency (Fig. 1). This is mainly because the

Corresponding author: Junhong Wang, jwang20@albany.edu

DOI: 10.1175/JTECH-D-20-0215.1

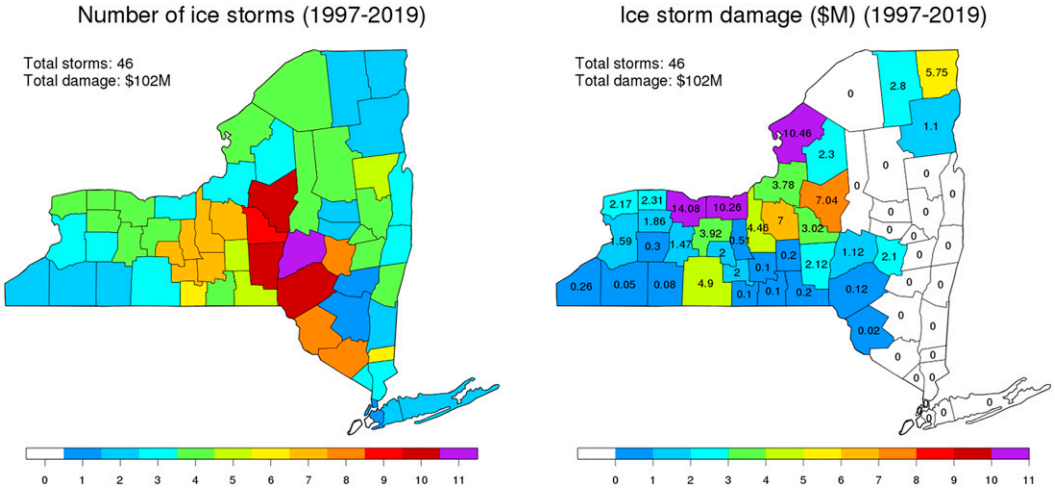

FIG. 1. Maps of (left) number of ice storms and (right) total damage for each county over New York from 1997 to 2019 as reported by NCEI.

damage figures are dominated by two ice storms. The 4–5 April 2003 ice storm was responsible for over $65 million of that year's total $67 million in winter weather-related damages. Two particularly severe events associated with this storm were due to a combination of ice and snow which fell together on a 19 countywide area for over 2 days, bringing down trees on homes, cars, electric lines, and other infrastructure. The second most devastating ice storm occurred in January 1998 across northern NYS and New England (DeGaetano 2000). A conservative estimate of total ice storm related damages exceeded $1 billion for New York, Maine, New Hampshire, and Vermont (DeGaetano 2000). Given the frequent occurrence of ice storms, the associated damages and high spatial variability in NYS as illustrated above, much-improved ice storm detection, monitoring and forecasting are needed both spatially and temporally.

A primary method of recording freezing rain events has been through the Automated Surface Observing System (ASOS). ASOS network has a freezing rain (FZRA) sensor dedicated to monitoring freezing rain. This sensor works by measuring the frequency of a vibrating probe; the vibrations slow down with the accretion of ice. This reduction in frequency is then recorded as freezing rain as long as the ambient temperature is below a certain threshold and snow is not the primary form of precipitation (NOAA 1998). The ASOS freezing rain report data are used for validation in section 3. Nevertheless, the limited spatial coverage provided by the ASOS network is a significant limiting factor in its utility. Only 49 ASOS sites are located across the entirety of New York State, and most of them are located at airports (Fig. 2), leaving large gaps of the state without direct sensor measurements of ice accretion. Instead, these areas are left reliant on local public reporting of ice storms and freezing rain, records that may be sparse at night and in low population areas and which are sometimes unreliable. This serious observational gap provides motivation to develop an automated sensor and/or tool to improve the resolution of freezing rain monitoring across New York State. The New York State Mesonet (NYSM; http://nysmesonet.org) consists of 126 standard environmental monitoring stations deployed statewide with an average spacing of 27 km (Fig. 2) (Brotzge et al. 2020). The primary goal of the NYSM is to provide high quality weather data at high spatial and temporal scales to improve atmospheric monitoring and prediction, especially for extreme weather events (Brotzge et al. 2020).

Given the substantial social, economic, and ecological impacts of ice storms and their frequent occurrences across New York, we set out to answer the following questions using the newly established NYSM. First, is it possible to detect icing

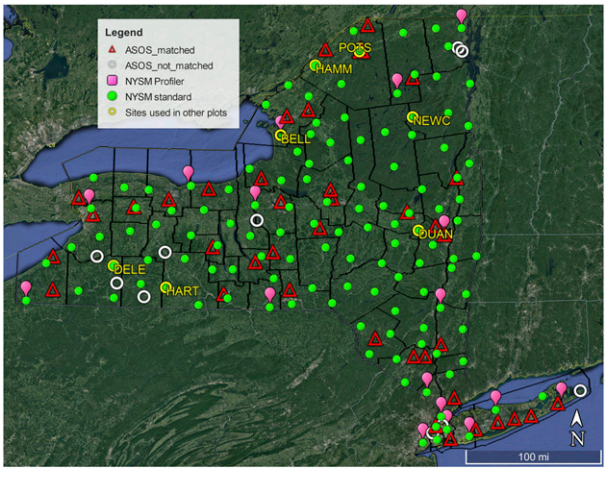

FIG. 2. Map of 126 NYSM standard sites (green dots) and 17 profiler sites (magenta balloons), and ASOS sites with (red triangles, 39) and without (white circles) matched NYSM sites. Yellow circles with site names denote sites used in Fig. 3 (HART), Fig. 4 (DUAN), Fig. 7 (NEWC), Fig. 14 (POTS), Fig. 17 (DELE, HAMM, and NEWC), and Fig. 18 (BELL).

conditions utilizing the NYSM? If so, can this icing detection be automated with minimal false alarms? Could refined climatology of freezing rain help improve the forecasting of ice storms? A limited study was conducted to answer these questions. The NYSM data and icing detection algorithm are described in section 2. The algorithm and detected freezing rain events for last four winters (2017–21) are validated against the ASOS data at collocated stations in section 3. A case study is reviewed in section 4 to demonstrate the validity of the methodology and highlight the added value from NYSM data for understanding freezing rain impacts and providing freezing rain situational awareness for warnings and emergency management. Conclusions are discussed in section 5 along with a look ahead to future work.

2. Data and methodology

a. NYSM data

The NYSM offers a solution to the spatial coverage problem associated with ASOS (Fig. 2). With 126 standard stations deployed across New York State's 10 distinct climate regions, with an average displacement of 27 km between stations, the NYSM is a valuable asset in analyzing past and ongoing weather and climate (Brotzge et al. 2020). A standard NYSM station provides 5-min measurements of all standard meteorological variables above and below the ground and additional parameters (snow depth, solar radiation, and soil temperature and moisture). In addition, a camera is installed at every site to provide coincident images of environmental conditions. All data including images are collected, quality controlled, and disseminated every 5 min in real time. The NYSM also operates a specialty network of 17 ''profiler'' stations (http://nysmesonet.org/networks/profiler). Profiler sites deployed across New York State are composed of lidar and microwave radiometer (Fig. 2). The profiler data provide continuous measurements of boundary layer thermodynamic and dynamic profiles, valuable for studying the freezing rain formation processes (e.g., Rauber et al. 2000). Nevertheless, there is not a dedicated freezing rain sensor installed at any NYSM station, nor is there any plan in the near future to deploy one in the NYSM.

To aid with data quality control, redundant measurements are collected for temperature and wind. Wind speed and direction are measured at 10 m AGL from two independent sensors: the R. M. Young wind propeller (Model 05103) and the Lufft two-dimensional sonic anemometer (v200A). The codeployment of these two sensors provides a unique opportunity to evaluate the performance of the sensors, quality control the data, and fill data gaps when one sensor fails. Generally, the two sensors agree with one other within 1 m s^{-1} (Fig. 3). The propeller generally reports a slightly lower wind speed due to a damping effect, i.e., frictional effects slow the propeller from turning. The percentage magnitude of the underestimation decreases with wind speed as the mechanical momentum overcomes frictional and other resistive forces

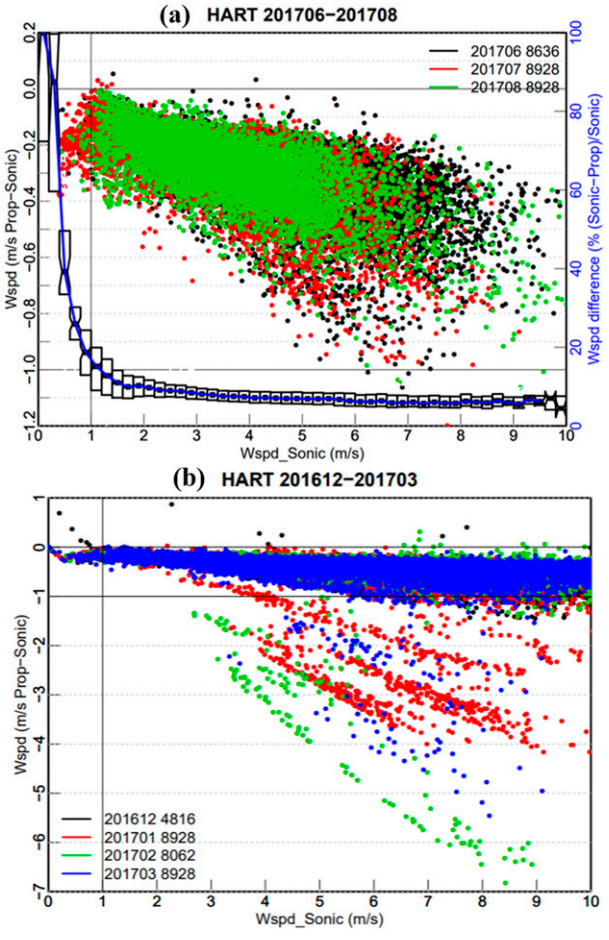

FIG. 3. Wind speed differences (propeller − sonic; in m s^{-1}) as a function of sonic wind speed (in m s^{-1}) (a) from June to August 2017 and (b) from December 2016 to March 2017 at Hartsville (HART) site. Different colors represent different months. The numbers in the legend represent total number of data points. Note that the scale for the *y* axis for the top and bottom panels is different. The boxplot in (a) is the relative wind speed difference [(sonic − propeller)/sonic in % using right *y* axis] for all 3 months.

(Fig. 3a). However, larger wind speed differences between the propeller and sonic anemometers are often reported during freezing rain or even wet snow conditions as shown at the Hartsville (HART) site during winter 2016/17 (Fig. 3b). The propeller develops a coating of ice or wet snow, which slows and eventually stops the blades from turning. As one example, data are shown from 17 January 2017 at the Duanesburg (DUAN) site located in the Mohawk River valley (Fig. 4). An NYSM technician visited the site the following day and found that the tower was covered in an approximate 0.25-in. layer of ice, which was nicely captured by our camera (Fig. 4a). The propeller completely stopped spinning starting at 2130 UTC 17 January and recovered at 1900 UTC 18 January only after the technician cleared the ice from the propeller (Fig. 4b). This example illustrates the utility of cameras to detect icing conditions remotely. Unfortunately, at this time

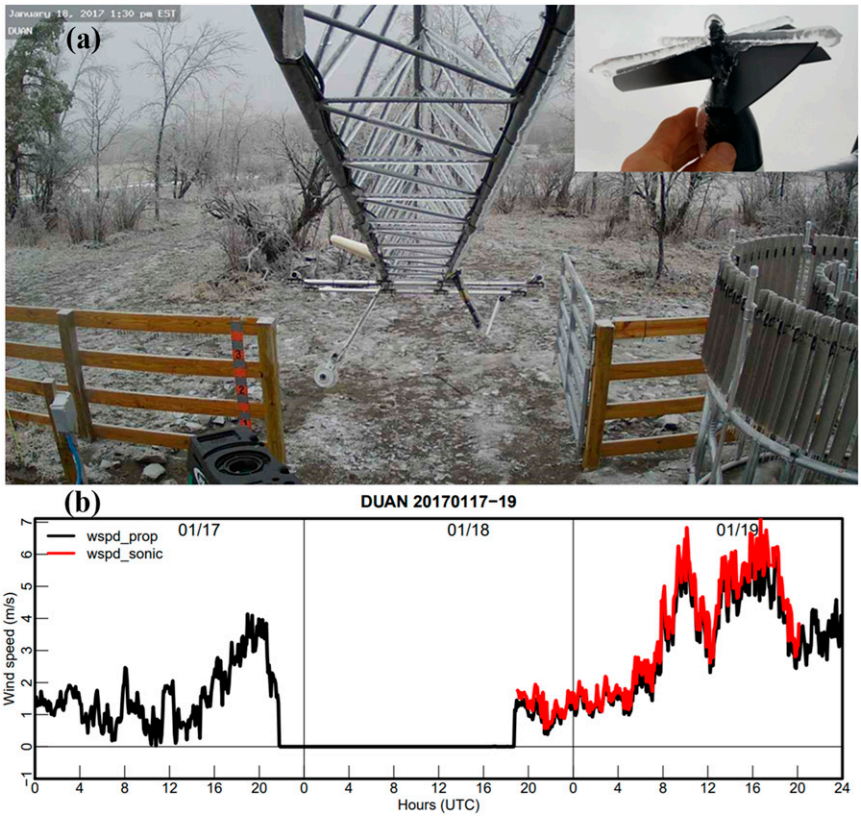

FIG. 4. (a) Duanesburg (DUAN) site photo taken at 1300 EST (1830 UTC) 18 Jan 2017 by our camera when our technician lowered the tower. The inserted photo shows an iced propeller and (b) time series of 5-min wind speed and gust during 17–19 Jan 2017 at DUAN as measured by the propeller and sonic anemometers.

the sonic anemometer was not working prior to 18 January due to an unrelated electrical issue.

The challenge of measuring winds during snow or icing conditions using a cup or propeller anemometer is well known, and no sound technological solutions are available to resolve the issue (Fiebrich 2003; Makkonen et al. 2001; Sonmez et al. 2005; Fiebrich et al. 2010). Unfortunately, due to the difficulty of identifying wet snow/icing conditions automatically, all impacted propeller wind data must be flagged manually. Prior studies have used comparisons between 2- and 9-m wind measurements, identifying unchanging wind speed or direction or visual quality control (QC) to flag affected data (Sonmez et al. 2005; Fiebrich et al. 2010). During winter, the wind comparisons between the propeller and sonic anemometers are closely monitored for freezing rain and wet snow conditions, and the false data are manually flagged in a timely fashion. Such manual QC is time consuming and tedious, but it motivated the QC team to turn an apparent "error" in the data to a "signal" for detecting icing. The difference in wind speed between the two anemometers, especially when combined with additional NYSM data, can yield an automatic tool for detecting icing conditions.

b. *Manual detection method*

As described above, during wet snow or icing conditions the propeller anemometer can accrete frozen water on the blades causing it to rotate more slowly than it should, or even stop completely. In contrast, the sonic anemometer is largely unaffected by icing especially when its internal heater is turned on. Thus, during these winter conditions the sonic anemometer acts as a reference, helping to identify instances in which the propeller wind speeds drift from the sonic value by a given threshold; based on experience and analysis of wind speed differences (Fig. 3), we have found that a difference $> 1\,\mathrm{m\,s^{-1}}$ is a good indicator of wet snow or freezing rain. To differentiate between wet snow and freezing rain, other NYSM data are used, such as snow depth and camera images. Manual and automatic approaches are developed and are described in detail below.

The manual methodology was developed by observers within the NYSM Operations Center based on repeated observations from across the NYSM as a part of its manual data QC process (Brotzge et al. 2020). The method is summarized in Fig. 5 with a focus on flagging erroneous wind data. The process begins with visually examining the wind speed differences for two days for all 126 stations organized by climate region (Fig. 6 for the ice storm on 14–16 April 2018). If there are spatially and temporally coherent areas of wind speed differences exceeding $1\,\mathrm{m\,s^{-1}}$ (blue-colored areas in Fig. 6), the process of investigation starts by following the steps listed in Fig. 5. The 2-day

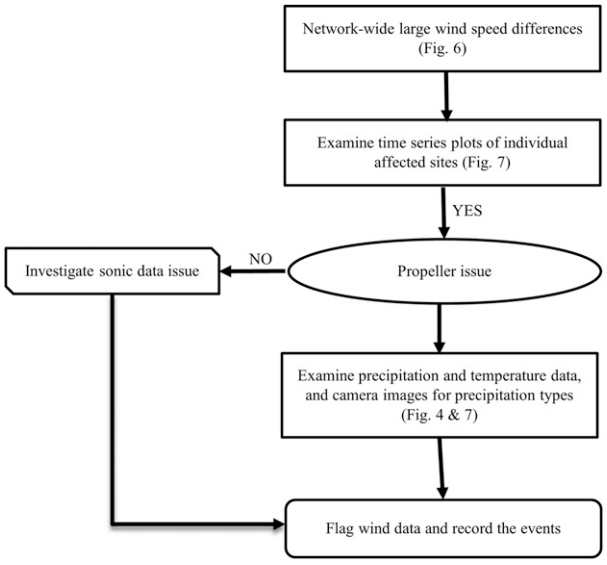

FIG. 5. Schematic diagram of the manual method for flagging wind data for icing and wet snow conditions (see the text for details).

time series of all variables at affected sites are inspected to find out which anemometer has the issue [see an example for Newcomb (NEWC) in Fig. 7]. Figure 7 shows that NEWC propeller anemometer stopped working at 0700 UTC 15 April and recovered around 1630 UTC 16 April when the air warmed up (Fig. 7b). The below-freezing temperature, precipitation accumulation (Fig. 7a) and camera images all confirmed that freezing rain caused icing buildup on the propeller. Propeller data were flagged for impacted sites and time periods, and the events were documented in a spreadsheet including the season event number, affected sites, starting and ending times for each site, affected anemometer, and weather type (ice or wet snow). The camera at NEWC nicely captured the bushes ''waking up'' from the freezing rain around 1230 EDT when the temperature climbed up above ~0.5°C (see the video https://operations.nysmesonet.org/public/references/20201215_icing_detection/newc.mp4 and Fig. 7b).

c. *Automated detection method*

The automated algorithm requires quantitative thresholds for the wind speed difference and air temperature, which are described in detail below. Furthermore, we distinguish between two stages of icing conditions: active freezing rain (AFR) and frozen surface (FS). The AFR (FS) is defined as when the propeller is possibly coated with ice with (without) a detectable amount of falling freezing rain recorded during the last hour. The threshold for ''detectable amount'' of hourly precipitation accumulation is defined as the minimum hourly threshold of the Pluvio rain gauge (0.05 mm). The hourly snowfall, as derived from the NYSM SR50A snow depth measurement, is used to exclude cases in which wet snow caused the propeller anemometer to slow down. The threshold for hourly snowfall is selected as half of the accuracy of the SR50A measurement (5 mm or 0.2 in.); 0 mm is not used because there might be a small snow depth increase during freezing rain.

The wind speed difference and temperature thresholds were derived by analyzing manually detected icing events during the winter of 2017/18. Figure 8a shows the frequency distribution of propeller wind speeds compared to sonic wind speeds recorded during freezing rain events in the 2017/18 winter. The propeller recorded 0 m s^{-1} about a third of the time (Fig. 8a). This reinforces the fact that the propeller completely freezing (stopping) is not a rare or insignificant event. Note the leftward shift of the distribution of propeller wind speeds compared with the sonic wind speed distribution (Fig. 8a). The frequency distribution of wind speed differences as reported during icing events shows a clear peak at 1 m s^{-1} (Fig. 8b). It was also found that during some events the sonic anemometer sustained wind speed remained below 1 m s^{-1} while the propeller was frozen. In these situations, a wind speed difference of less than 1 m s^{-1} was reported even though icing conditions were still present. This suggests that the 1 m s^{-1} threshold could underreport icing conditions when the sonic reports <1 m s^{-1} wind speed and the propeller has 0 m s^{-1}.

Another noteworthy feature is seen in the distribution of air temperatures observed during the icing events. A sharp temperature threshold limits icing events to 1°C or below (Fig. 9). As temperatures approach 1°C, object skin temperatures can remain below the air temperature, meaning skin temperatures could remain at subfreezing allowing for ice accumulation if cooled liquid were to come in contact with that surface. At temperatures below 0°C, it can be seen that the distribution appears more normal with a gentle decrease in frequency as colder temperatures are reached (Fig. 9). With this gentler slope in mind, it is difficult to define a left bound on the temperature threshold partially because once the propeller is frozen, it will stay frozen as long as temperatures are below freezing point. The evolution of temperatures over the duration of icing events is also investigated by normalizing the time as 0 at the starting freezing point and 1 at the ending point. As an example, Fig. 10 shows the temperature profiles at nine stations across the Central Lake region for the 14–16 April 2018 ice storm. The ice storms begin with temperatures below freezing, become warmer with time, and then end with temperatures between 0° and ~2°C (Fig. 10). Ice on the propeller starts to melt once temperatures are above 0°C, but melting takes time and depends on the ice thickness and the environmental conditions. This explains the long tails of the above-freezing temperatures in Fig. 10. Note also that the ending time represents the time when the propeller is ice-free enough to begin spinning again rather than the stopping time of the active freezing rain, which is much earlier. Figures 9 and 10 imply that it is difficult to select a fixed temperature threshold to fit all conditions. Prior studies concluded that the phase of precipitation (rain, snow, or ice) depends on various factors (e.g., temperature, humidity, and pressure) (Dai 2008; Ding et al. 2014; Jennings et al. 2018). A summary of nine schemes for discriminating precipitation type (Table 1 in Ding et al. 2014) concludes that the air temperature threshold for freezing rain ranges from −5.5° to 4°C. Prior studies further confirm the challenge of selecting a

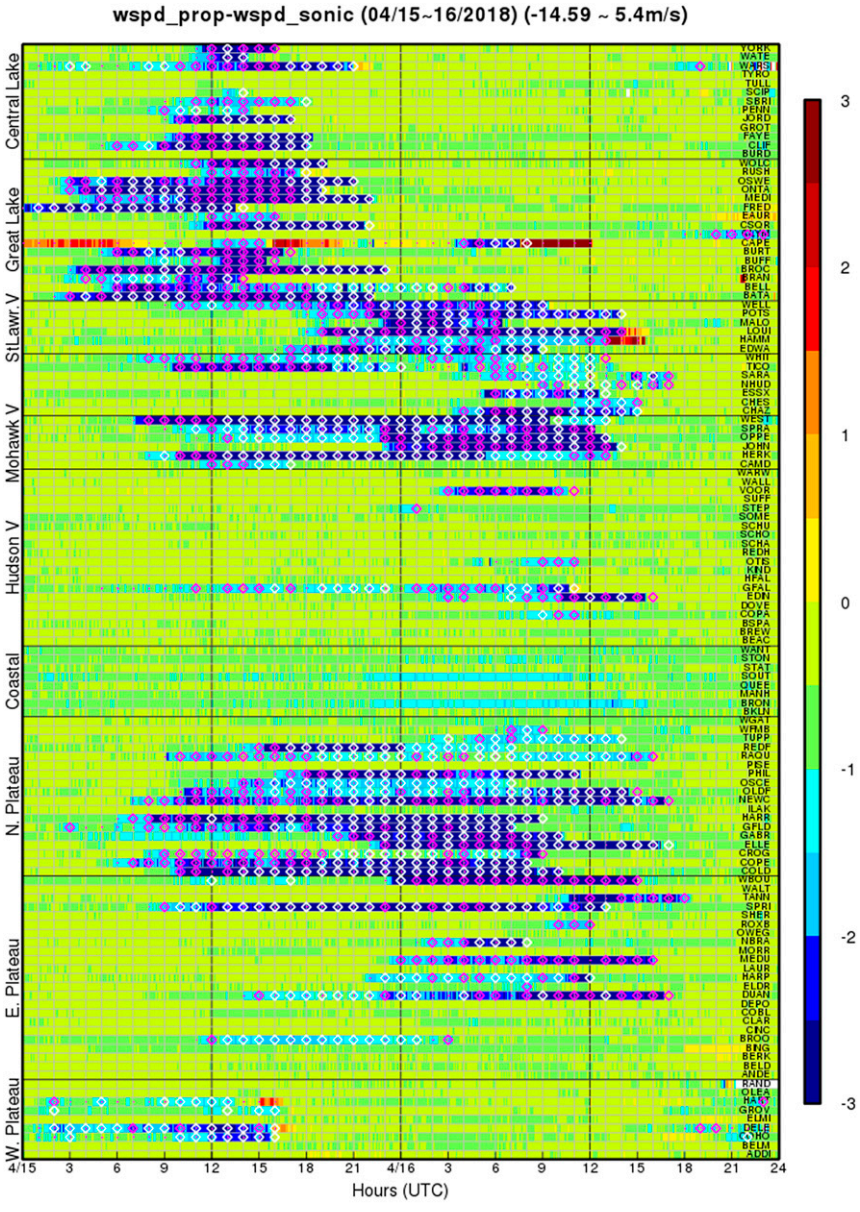

FIG. 6. The 5-min difference (m s^{-1}; color filled) in wind speed between the propeller and sonic anemometers are shown at 126 stations (y axis) for 15–16 Apr 2018 (UTC; x axis); each row represents a different station, and stations are grouped by their climate division. The magenta dotted area shows that the propeller data were manually flagged. Hourly active freezing rain (magenta diamonds) and frozen surface conditions (white diamonds) derived from automated method are also shown.

single fixed temperature threshold. Based on Figs. 9 and 10 for our particular application, a range of −5° to 2°C temperature is selected for active freezing rain, and a threshold of temperatures below 2°C for frozen surfaces.

One goal of the automated method is to produce a map of AFR and FS sites every hour in real time. Five variables are used: propeller and sonic wind speeds, hourly average temperature, hourly precipitation accumulation, and hourly snowfall. Five-minute propeller and sonic wind speeds and their differences are analyzed hourly to calculate the duration during the previous hour when the wind speed difference (propeller − sonic) is $<-1\,m\,s^{-1}$ or the propeller wind speed is $0\,m\,s^{-1}$. The requirements for AFR and FS are detailed in Table 1.

The detected AFR and FS conditions using the automated method for the 14–16 April 2018 ice storm are shown in Figs. 6, 7, and 11. Figure 6 shows that the spatial coverage and temporal evolution of icing conditions (combined AFR and FS) generally agree well with that from the manual method.

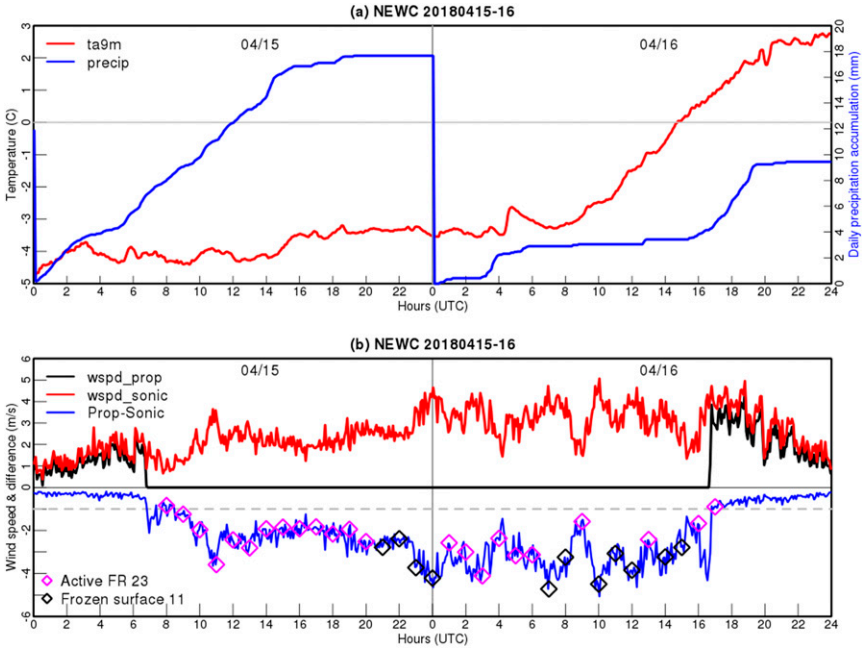

FIG. 7. Time series of 5-min (a) temperature at 9 m (red line) and daily accumulated precipitation (blue line) and (b) wind speeds from two anemometers (black and red lines) and their differences (blue line) at NEWC on 15–16 Apr 2018. Hourly active freezing rain (magenta diamonds) and frozen surface conditions (black diamonds) are also shown on the wind speed difference line in (b).

However, the automated method intermittently failed during the manually detected icing period when the wind speed difference is around $-1\,\mathrm{m\,s^{-1}}$. For those cases, the manual method would take into account overall temporal variations of wind speed difference and visually determine the starting and ending time (see Fig. 7). But the automated method is constrained by the thresholds in Table 1 and ignores temporal connections. There also exists ambiguity between AFR and FS and the delay in detecting AFR, which can be explained by an example in Fig. 7 for NEWC. The automethod detects the first AFR during ~0700–2200 UTC 15 April 2018, then about 4 h of the FS condition and another AFR event during ~0000–0600 UTC 16 April followed by the FS condition until 1700 UTC (Fig. 7). But the start of the first AFR event likely occurs before that since there has to be enough ice accumulated on the propeller to stop it spinning. During the second FS period (0700–1700 UTC 16 April), there are four points labeled as AFR due to the light precipitation accumulation (Fig. 7). Figure 11 shows statewide maps of icing conditions at four times during the 14–16 April 2018 ice storm. It shows spatially and temporally coherent structures of AFR and FS across the state and the transition from AFR to FS in the Tug Hill regions from 1400 to 2200 UTC 15 April (Fig. 11). The automated method can be further refined by adjusting the thresholds used in Table 1 and taking into account temporal and spatial changes of AFR and FS conditions.

3. Comparisons with ASOS

The ASOS FZRA report is based on measurements from the ASOS freezing rain sensor, the ambient temperature, and the reporting scheme of the ASOS Present Weather Report (NOAA 1998). The FZRA algorithm is run every minute using data collected during the last 15 min (NOAA 1998). Freezing

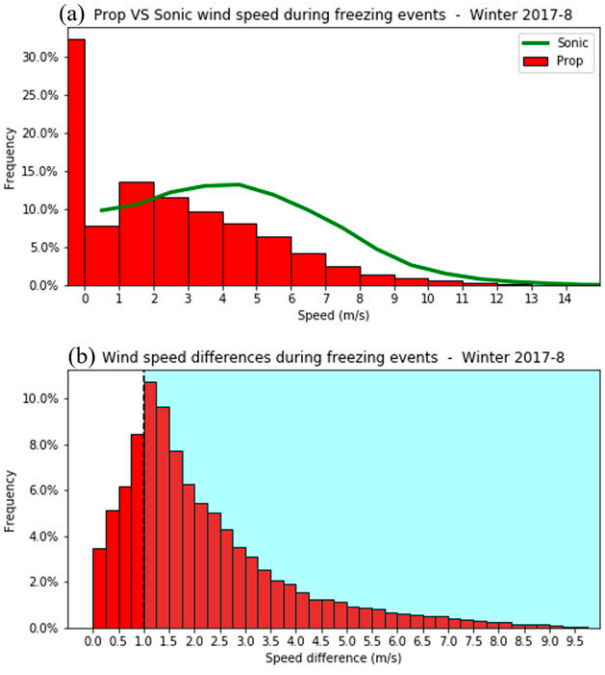

FIG. 8. (a) Frequency distributions of wind speeds (in $\mathrm{m\,s^{-1}}$) from the propeller and sonic measurements and (b) wind speed differences (sonic − propeller; in $\mathrm{m\,s^{-1}}$) during icing events for the winter of 2017/18.

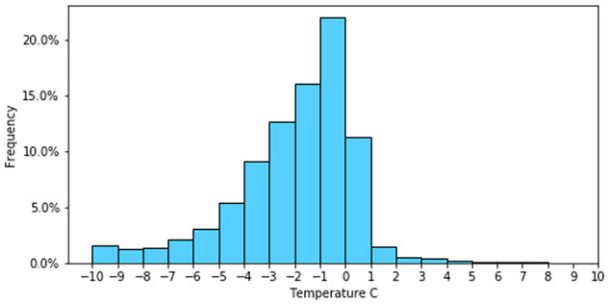

FIG. 9. Frequency distribution of temperature at 9 m during all icing events in winter 2017/18.

rain is reported for the current minute if required conditions are met. Otherwise, it is set to indicate a lack of freezing precipitation. The ASOS FZRA reports, especially from augmented ASOS stations, are found to be consistent with manual observations in the frequency of occurrence (Reeves 2016). For this study, 5-min ASOS FZRA data for the last four winters (2017–20) are used to compare with active freezing rain events detected by the automated detection method described in section 2. The ASOS 5 min data in NYS are downloaded from 1 November 2017 to 18 April 2021 for each winter month (November to April); these data were retrieved from the Iowa State University website (https://mesonet.agron.iastate.edu/request/download.phtml?network=NY_ASOS). Thirty-nine stations out of a total 49 ASOS stations in NYS are located within 30 km horizontally and 80 m in elevation of an NYSM site and thus are selected for this study (Fig. 2). ASOS variables include Present Weather Codes (PWC), the ice accretion over 1 h, and air temperature.

It is not straightforward to compare the freezing rain detected by ASOS and our method because of the episodic nature of freezing rain, differences in sampling (1 min for ASOS vs 1 h for NYSM), spatial matching, strength and weaknesses of each method, and other factors. The following steps are taken to compare them.

1) The first step is to group the 4-yr data into episodes for each dataset (ASOS and NYSM). We use the similar definitions of ''episode'' and ''event'' as NCEI. An ''episode'' is defined as a period with sequential ASOS FZRA or NYSM AFR reports. An ''event'' is referred as to each site within each episode. The number of events for each episode would be the number of sites with FZRA. An episode number is assigned for each data record. The gap between two consecutive episodes has to be at least 6 h. The NYSM automated detection method is run hourly for each winter for 39 matched stations to identify AFR and FS conditions. NYSM FS records are not considered here since they are not detected by ASOS.
2) The second step is to calculate the starting and ending times of the AFR and the duration of each event for both ASOS and NYSM data. The frequency distribution of freezing rain durations derived from the two datasets (Fig. 12) agree with each other remarkably well and are consistent with prior studies (e.g., Cortinas et al. 2004; McCray et al. 2019). More than 30% of freezing rain events last less than 1 h, and

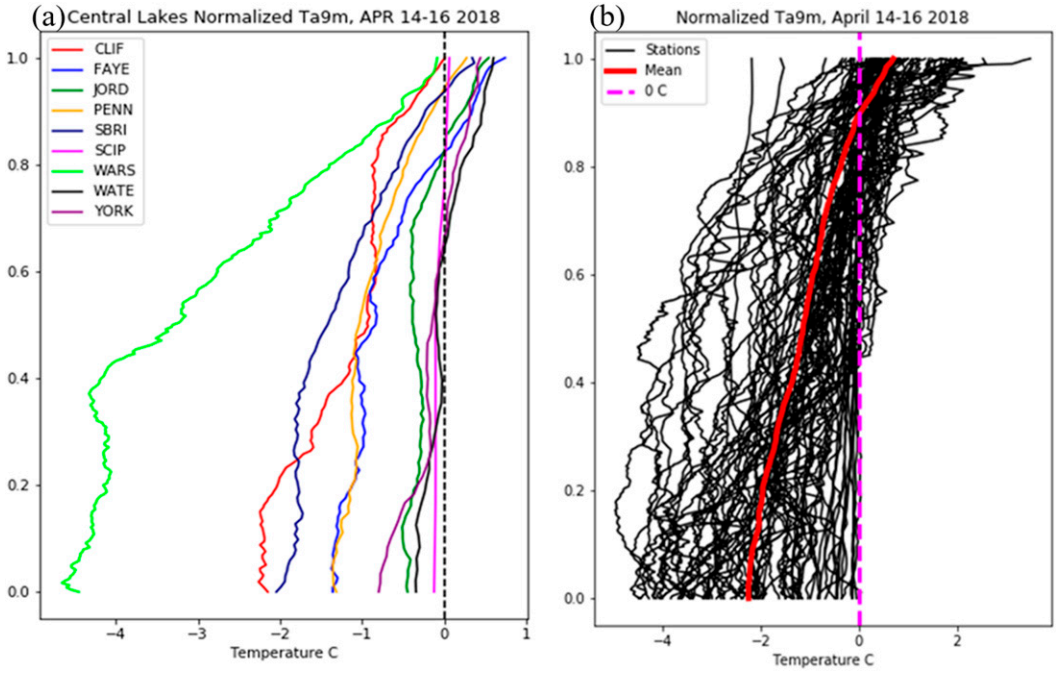

FIG. 10. Plot of 9-m temperatures as a function of normalized time (see the text for details) for (a) nine stations across the Central Lake region and (b) all stations during icing events for the 14–16 Apr 2018 ice storm. The mean temperature profile averaged for all stations is shown as a red line in (b).

TABLE 1. Requirements for active freezing rain and frozen surface for the automated method.

Criterion	Active freezing rain	Frozen surface
Duration of wind speed differences $< -1\ m\ s^{-1}$ or propeller wind speed $= 0\ m\ s^{-1}$	>30 min	>30 min
Temperature (T)	$-5°C < T < 2°C$	$T < 2°C$
Hourly snowfall (HS)	HS < 5 mm	HS < 5 mm
Hourly precipitation accumulation (HPA)	HPA ≥ 0.05 mm	HPA < 0.05 mm

the frequency decreases exponentially with increasing duration (Fig. 12). The NYSM tends to detect more longer-duration events (≥6 h) (Fig. 12).

3) The final step is to match and compare the ASOS and NYSM event statistics spatially and temporally. A total of 110 and 80 freezing rain episodes were detected by ASOS and NYSM, respectively, during the period of study. ASOS events lasting shorter than 1 h (36%) are excluded from the comparison because of hourly resolution of NYSM AFR data. Fifty percent of NYSM episodes have 1-h total duration (including all sites) or only include one or two stations. They are most likely to be false, local, or isolated cases, and so are removed from the comparison. The matched episodes mean that there is at least some overlap in time between the ASOS and NYSM records. Then within each episode, ASOS and NYSM sites are matched (Fig. 2). Figure 13 shows comparisons of the start and end times and durations of 91 matched events from 40 matched episodes.

For all 498 events NYSM detected in Fig. 12, 16% of them are matched by ASOS. In other words, the NYSM overall false alarm rate is 84%. After step 3 described above, the probability of detection (POD) for NYSM events within matched episodes increase to 38%, and the false alarm rate is 62%. Those NYSM "false alarm" events are a result of limitations in both datasets. Many of NYSM's false alarm events occurred in a combination of very light winds, cold temperatures, and wet, light snow. Wet snow can stick on the propeller and cause it to slow or stop, but in these situations, the event was labeled as ice and not snow because the snow depth accumulation was less than the snowfall threshold of $5\ mm\ h^{-1}$. The light wind also makes the propeller more susceptible to wet snow since the propeller cannot efficiently get rid of the snow accumulated on it. For the rest of NYSM's false alarm events, ASOS often had unknown

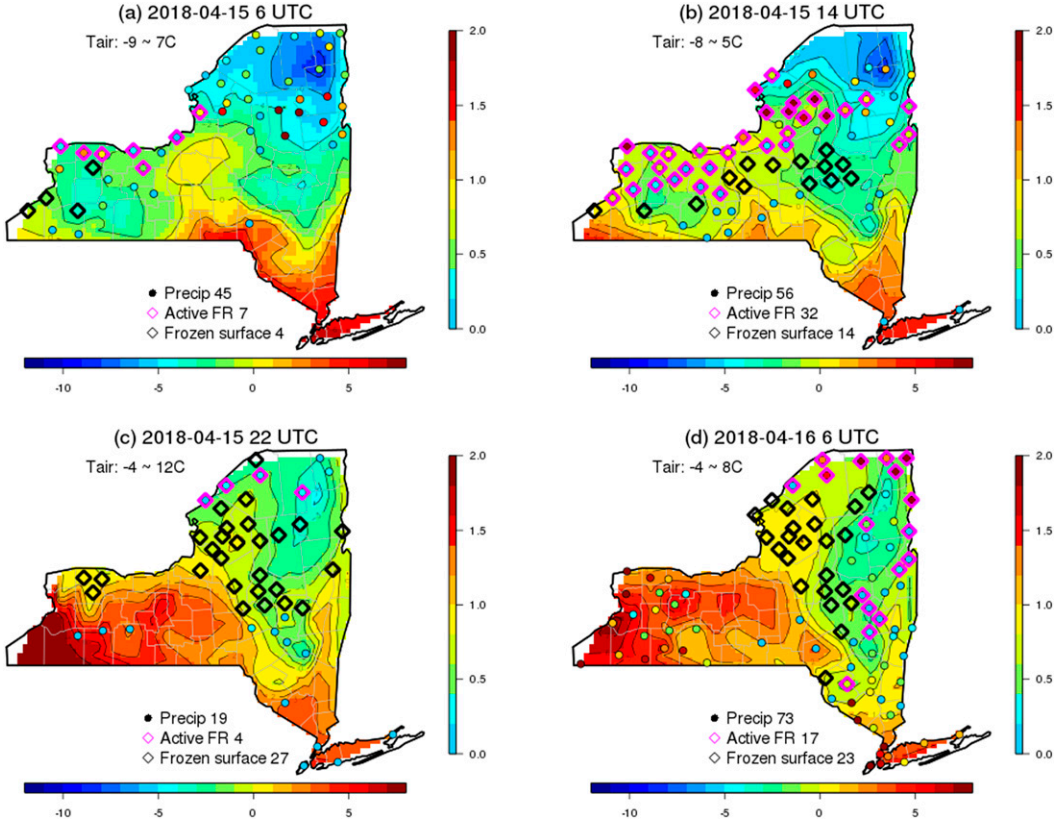

FIG. 11. Sites with precipitation (colored by precipitation accumulation in mm during last hour; left color bar), active freezing rain (magenta diamonds), frozen surface conditions (black diamonds), and maps of 9-m temperatures (color filled in °C; bottom color bar) at (a) 0600, (b) 1400, and (c) 2200 UTC 15 Apr and (d) 0600 UTC 16 Apr. Numbers of precipitating, AFR, and FS sites are shown in the legends.

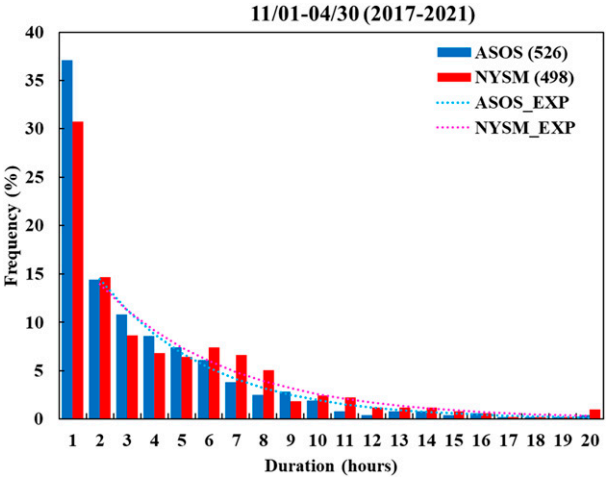

FIG. 12. Frequency distribution of durations of all freezing rain events detected by ASOS and NYSM. The dotted lines are exponential fitting to the events with duration larger than 1 h.

precipitation (UP), light rain, or light snow. Note that ASOS PWC follows the hierarchy of liquid–freezing–frozen, in ascending order of priority. Only the highest priority precipitation phenomena observed is reported at any one time (i.e., ASOS does not report mixed or multiple precipitation types). As an example in Fig. 14 for the ice storm on 14–16 April 2018, the ASOS station near NYSM Potsdam (POTS) showed no measurable ice accretion and reported unknown precipitation, mist or missing during the NYSM-detected AFR period. However, the NYSM camera confirmed the AFR presence. This example demonstrates that some of NYSM's ''false alarm'' events are real AFRs, but are missed by ASOS.

Figure 13 shows the comparisons of starting and ending times and durations of freezing rain events as detected by both the NYSM and ASOS networks. The starting and ending times shown are the hours from 0000 UTC on the earliest date of matched NYSM and ASOS events. There are good agreements in the starting and ending times between the two systems with correlation coefficients of 0.93 and 0.92, respectively. The NYSM freezing rain events generally start and end later, but most of them are within 5 h of the ASOS times (Figs. 13a,b). NYSM's later starting time is expected since the propeller does not start to slow down until enough ice has built up on the blades. The later ending time is possibly a result of the residual ice coating remaining on the propeller after the freezing rain stops; light or drifting snow detected by the Pluvio gauge is recorded as precipitation but without showing detectable snow accumulation. It should be noted that the NYSM method outputs hourly freezing rain reports. The starting and ending times can be anytime within that hour. The midpoint of the hour is used in Fig. 13. The ASOS FZRA reports are provided every 5 min. Differences in sampling resolution contribute to the uncertainty. The duration comparison still shows significant correlations in spite of the large scatter (Fig. 13c). Figure 13 validates our automated algorithm by

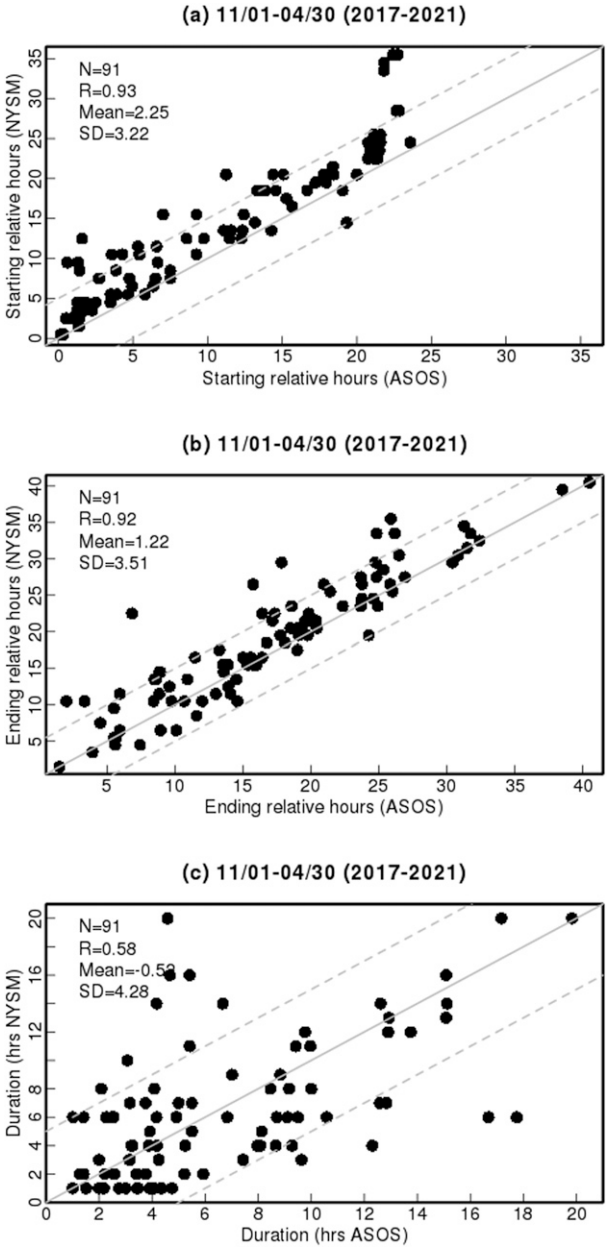

FIG. 13. Scatterplots of (a) starting and (b) ending times and (c) duration of 91 matched freezing rain events. The legend shows the number of cases (N), correlation coefficient (R), and mean (M) and standard deviation of the differences (NYSM − ASOS). The solid gray line is one-to-one line. The dashed gray lines are ±5 h from the one-to-one line.

detecting not only the occurrence of active freezing rain events but also their timing.

4. Ice storm on 14–16 April 2018

To evaluate the effectiveness of the icing detection methods, the 14–16 April 2018 ice storm was selected as a case study.

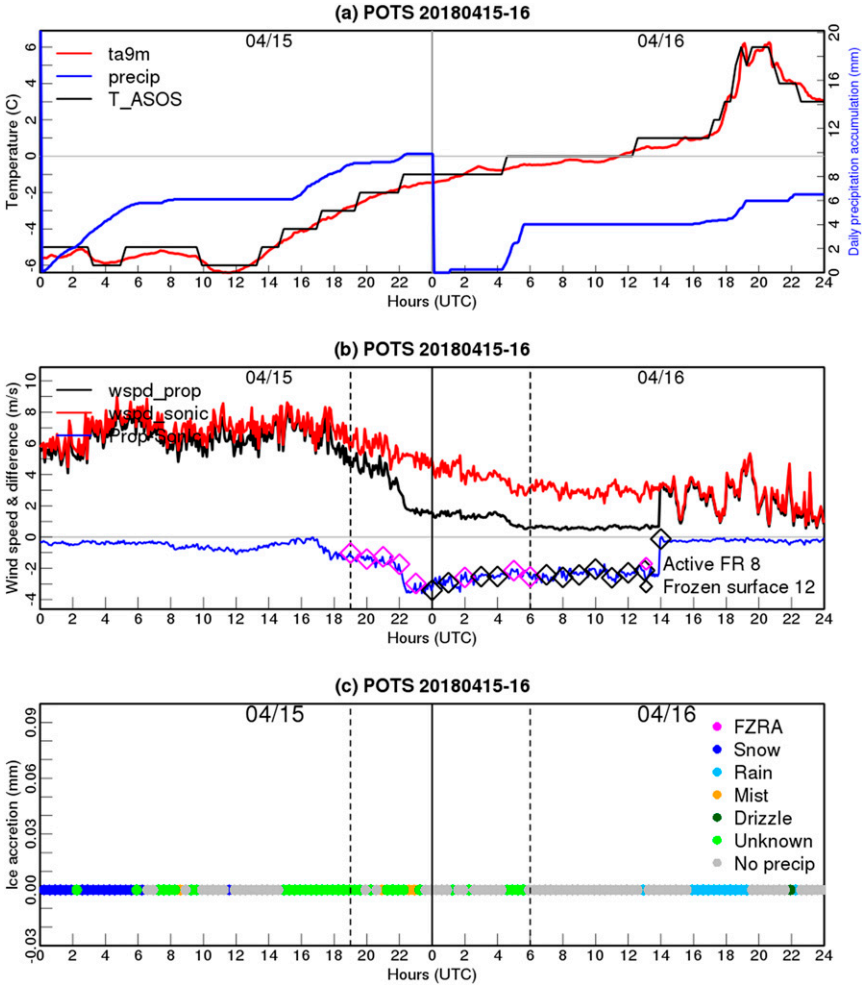

FIG. 14. Time series of (a) NYSM 9-m temperature (red line) and daily accumulated precipitation (blue line), and ASOS 2-m temperature, (b) NYSM wind speeds from two anemometers (black and red lines) and their differences (blue line), (c) ASOS hourly ice accretion (black bar) with dots for precipitation types at POTS on 15–16 Apr 2018. Hourly AFR (magenta diamond) and FS (black diamonds) are also shown in (b). Vertical dashed black lines in (b) and (c) are starting and ending times of AFRs detected by NYSM.

This case was chosen because it was the largest freezing rain event of the year for New York State. It affected 24 counties and resulted in $226,000 in damage (NCEI 2019). Several areas saw nearly an inch of sleet combined with around one-half inch (13 mm) of freezing rain. This resulted in thousands of power outages and substantial tree damage. Freezing rain was identified at 74 NYSM sites through the duration of the storm based on a manual review.

The 14–16 April 2018 winter storm was synoptically driven, originating to the west of the Rockies as a small surface low pressure center upstream of a standard trough at 1200 UTC 12 April. It represents one of two typical synoptic setup for freezing rain: warm front or occlusion sector of a cyclone (Rauber et al. 2001; Degelia et al. 2016). As the storm slowly tracked east, cold dense air from the north flowed down into the Northeast while very moist and warm air from the Gulf of Mexico advected north and flowed up and over the stationary boundary. As a result, the classical melting process occurred and generated the freezing rain (Zerr 1997; Huffman and Norman 1988; Degelia et al. 2016).

According to the NCEI archives, there were two rounds of mixed winter precipitation that moved across the area during 14–16 April 2018. NCEI recorded two episodes, an ice storm concentrated in the Great Lakes, Central Lakes, and Tug Hill regions and a winter storm in the Mohawk valley and Capital District (Fig. 15). The ice storm started in the evening of 14 April and ended in the afternoon of 15 April. The winter storm lasted from midnight of 14 April to the afternoon of 15 April, but led to high winds in Washington, Rensselaer, and southern Herkimer counties from early morning to early

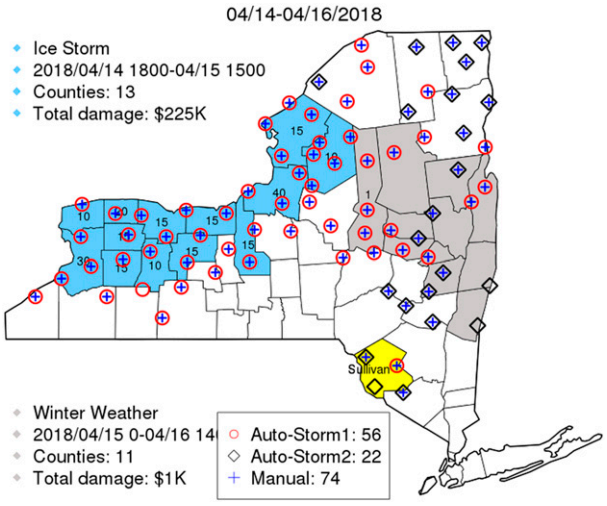

FIG. 15. Counties impacted by the ice storm from 1800 EST 14 Apr to 1500 EST 15 Apr (light-blue-shaded counties) and the winter weather from 0000 EST 15 Apr to 1400 EST 16 Apr (gray-shaded counties). The damage in thousands of dollars for each county is also labeled. Three symbols represent icing NYSM sites detected by the manual method (blue plus) and the automethod before and after 1500 EST 15 Apr ("Auto-Storm1" and "Auto-Storm2"). Sullivan County is highlighted in yellow.

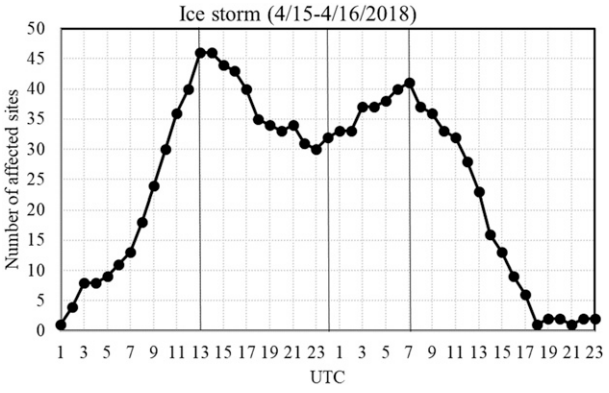

FIG. 16. Hourly number of affected icing sites from 0100 UTC 15 Apr to 0000 UTC 16 Apr. Three vertical black lines denote two times when maximum values occur and 0000 UTC 16 Apr to separate the 2 days.

afternoon of 16 April. The ice storm accounted for $225,000 of the storm total $226,000 in damage.

The impact areas of this ice storm as reported in NCEI and as detected by our manual and automated methods are shown in Fig. 15. As expected, the automated method agrees with the manual method very well except for four stations. The hourly number of affected sites as detected by the automated method clearly separates the two storms as reported by NCEI with a maximum number of 46 sites at 1300 UTC 15 April associated with the first storm and then 41 sites associated with the second storm at 0700 UTC 16 April (Fig. 16). In Fig. 15, the autodetected stations are divided into the two events as identified by NCEI (before and after 1900 UTC 15 April). Our method detected the icing conditions (either AFR or FS) in all the affected counties as reported by NCEI and also agrees with NCEI on the time spans of the two storm systems (Fig. 15). However, NYSM also found icing conditions across a larger area than reported by NCEI, such as across the North Country (Saint Lawrence, Franklin, Clinton, and Essex counties) and some high elevation areas across the West and East Plateau regions (Fig. 15). We surmise that this is due to the fact that the NCEI under samples in areas of low population and for marginal or low-impact events, since NCEI storm reports are generated by local officials. Cameras at the four NYSM stations in Sullivan County all show that the ground was covered by a thin layer of ice/sleet on the morning of 16 April. However, reports from Sullivan County are absent in the NCEI database, possibly due to the negligible impacts observed there.

The NYSM camera network also aids with confirmation of icing conditions. Icing is identified visually from iced fences, ice-covered cameras, "sleeping" bushes that droop due to ice weighting and "awakening" bushes that spring back up after melting (Fig. 17). Time-lapse video of the 5-min images is helpful to monitor changes and to determine whether icing conditions are continuing or improving. Camera images are archived and can be easily replayed for past events using our online camera viewer. A number of studies have reviewed the adverse effects of ice storms on forests (e.g., Irland 2000), and cameras can be a valuable aid in evaluating the short-term and long-term damage of ice storms on forests. For example, a heavy ice storm (~1 in. liquid-equivalent precipitation) at the Saranac Lake station on 30 December 2019 placed a heavy load on trees, as seen at 0730 EST (see the video https://operations.nysmesonet.org/public/references/20201215_icing_detection/sara.mp4) and an immediate subsequent snow storm added additional weight. The foliage did not rebound until ~77 h later at ~1430 EST 2 January 2020 when the sun came out and warmed temperatures to above freezing.

Continuous thermodynamic profiles are valuable to identifying freezing rain soundings for both warm rain and melting processes (Rauber et al. 2000). The NYSM Profiler network provides continuous profiles of temperature, humidity, and wind from the ground to up to 10 km AGL every 10 min at 17 stations (Fig. 2). Figure 18 illustrates the usefulness of MWR data for icing conditions on 15 April 2018 at Belleville in the Great Lakes region (see Fig. 2 for location). The AFR phase identified by our automated method occurred during ~0600–1800 UTC (0200–1400 EDT) (Fig. 18b) and show a thick above-freezing layer aloft (yellow-contoured area) and a thin layer of freezing temperatures near surface during the same period in the MWR data (Fig. 18d). Frozen surface condition continued until 0700 UTC 16 April. The continuous MWR temperature profiles allow forecasters to monitor the evolution of this typical warm nose sounding for freezing rain formation quickly and permit timely and accurate ice storm warnings. The ice accretion and precipitation type at Watertown International Airport (ART) ASOS station (23 km from BELL) are shown in Fig. 18c. Both datasets detected the long-duration freezing rain event on 15 April although

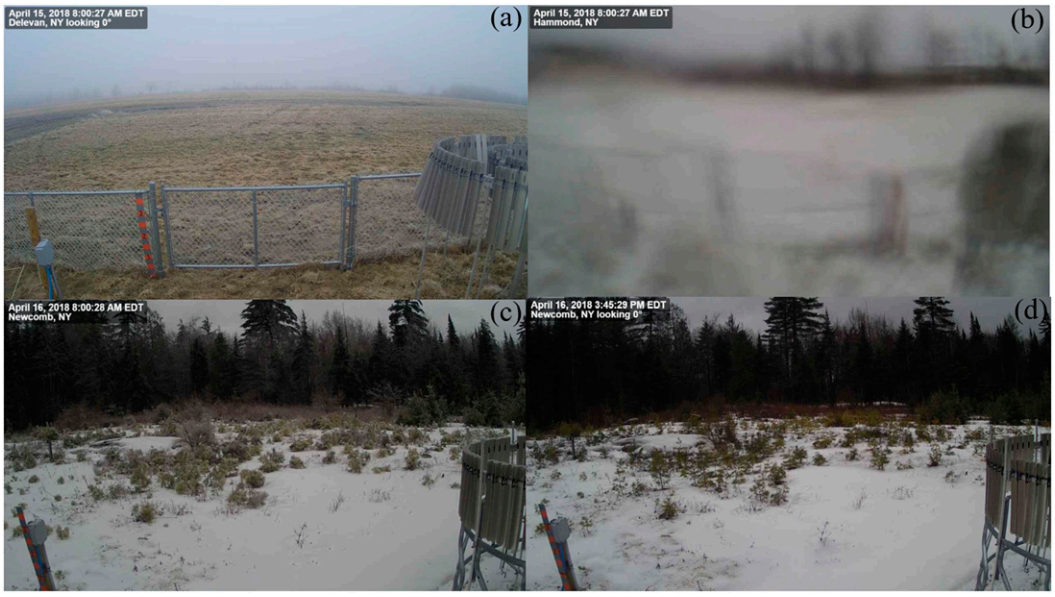

FIG. 17. Camera images (a) at DELE at 0800 EDT 15 Apr showing ice on the fence, (b) at HAMM at 0800 EDT 15 Apr with an ice-covered camera, (c) at NEWC at 0800 EDT 16 Apr with "sleeping" bushes, and (d) at NEWC at 1545 EDT 16 Apr with standing bushes after the ice melted away.

NYSM-detected AFR started two hours later. The second short-duration event between 0200 and 0400 UTC 16 April are present in both datasets, too. Another interesting feature shown in Fig. 18c is that the propeller stopped spinning at 1400 UTC when the hourly ice accretion increased to above 2 mm. This example quantitatively validates our automated method's capability of not only detecting the occurrence of AFRs but also determining their timings.

5. Conclusions

Ice storms pose a serious threat to safety and property, create hazardous conditions for travel, and can cause significant damage to forests. These winter events have the highest frequency in the northeastern United States, and specifically in New York State. During last 23 years (1997–2019) a total 46 ice storms were recorded by the NCEI database for NYS and caused $102 million in damage. In addition, icing conditions occurred in other storm types such as "winter storm" in the NCEI database which were not counted in this climatology.

Due to the frequency, severity, and spatial variability of freezing rain events throughout New York State, it is important to have a more accurate and reliable method to detect and monitor these events with better spatial resolution and in real time. With an average station spacing of 27 km throughout the state, the NYSM provides local surface data for such monitoring. By utilizing differences between its propeller and sonic anemometers, and with additional air temperature, precipitation, and snow depth data and camera photos, the NYSM can be a reliable tool for detecting icing conditions and distinguishing the initial active freezing rain (AFR) and frozen surface (FS) stages. An automated method is developed to produce hourly maps of sites with AFR and FS conditions in real time (Table 1). A site is deemed to be experiencing AFR if 1) the wind speed difference (sonic − propeller) is $>1\ \mathrm{m\ s^{-1}}$ or the propeller wind speed is $0\ \mathrm{m\ s^{-1}}$ for at least 30 min, 2) the average temperature during the hour is within −5° to 2°C, 3) total snowfall during the hour is less than 5 mm (0.2 in.), and 4) the hourly precipitation accumulation is more than 0.05 mm. The requirements for the FS are similar to that for AFR except that 2) the average temperature is less than 2°C and 4) the precipitation accumulation is less than 0.05 mm.

The automated method and detected AFR events for the last four winters (2017–21) are evaluated against the ASOS freezing rain data at collocated stations. The comparisons conclude that two datasets show consistent frequency distribution of freezing rain durations for all events identified by each dataset and starting and ending times for matched events. The case study for the ice storm of 14–16 April 2018 further confirms the automated method's capability to detect the AFRs and determine their timings. The comparisons also reveal strength and weakness of both NYSM and ASOS methods.

The high-impact ice storm of 14–16 April 2018 was investigated in detail and used to validate the manual and automatic methods. The affected areas as reported by NCEI were detected by the manual and automatic methods. Furthermore, NYSM expanded the spatial and temporal map of icing conditions in low population and less impacted areas. Since our technique better estimates not only the onset of freezing rain but also the longevity of surface icing conditions, this information can be used as an initial aid for identifying possible areas where dangerous road conditions and tree damage are occurring, and especially when camera images are utilized.

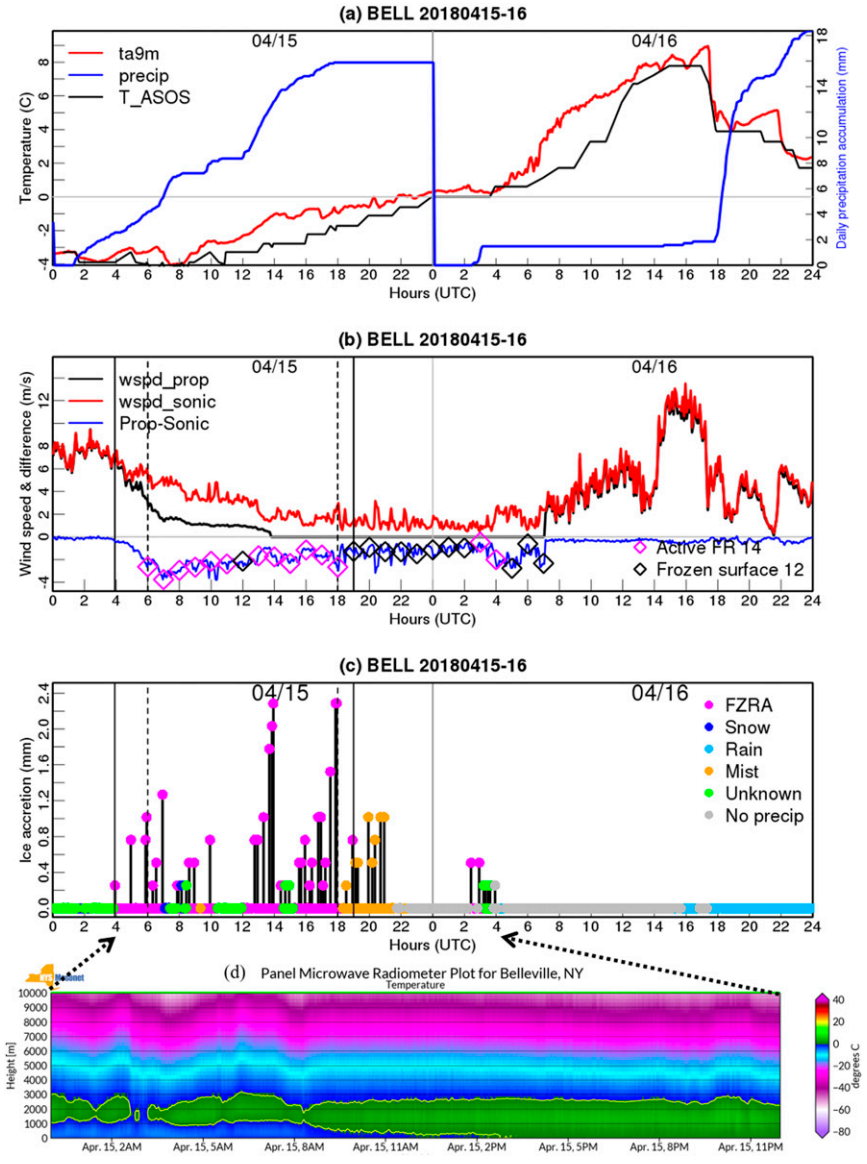

FIG. 18. Time series of (a) NYSM 9-m temperature (red line) and daily accumulated precipitation (blue line), and ASOS 2-m temperature, (b) NYSM wind speeds from two anemometers (black and red lines) and their differences (blue line), (c) ASOS hourly ice accretion (black bar) with dots for precipitation types at BELL on 15–16 Apr 2018, and (d) MWR-retrieved 10-min temperature profiles on 15 Apr 2018 (in EDT). Hourly AFR (magenta diamonds) and FS (black diamonds) are also shown in (b). Vertical black lines in (b) and (c) are starting and ending times of AFRs detected by ASOS (solid) and NYSM (dashed). Note that (a) and (b) are plotted against UTC time (4 h ahead of EDT).

Such data can be critical for transportation departments, insurance companies, and emergency managers. In the end, enhancing our ability to accurately indicate when and where ice storms are occurring and are persisting will help mitigate property loss and allow the public to make better informed decisions during such times.

Another important aspect of this work is the value of ground-based profiler networks such as the NYSM Profiler network for monitoring freezing rain conditions. The NYSM Profiler network can be used to monitor boundary layer profiles to alert users to favorable freezing rain conditions prior to the event (Fig. 18). Utilizing the microwave radiometer and lidar, vertical soundings can be generated every 10 min, meaning the formation, duration, and recession of freezing rain conditions can be tracked throughout the evolution of the storm in real time. These frequent profiles boost confidence in the warning process.

This work may be further improved by testing different thresholds for wind speed difference, temperature, precipitation,

and snowfall and incorporating temporal variabilities and spatial coherency into the automated algorithm. The false alarm events identified by comparing with ASOS data could be reduced by better handling light wind and wet snow conditions. While these methods are useful for detecting the *presence* of icing conditions (AFR and FS), future work will explore using NYSM data to estimate the amount of ice accretion during AFR.

Acknowledgments. This research is made possible by the New York State (NYS) Mesonet. Original funding for the NYS Mesonet was provided by Federal Emergency Management Agency Grant FEMA-4085-DR-NY, with the continued support of the NYS Division of Homeland Security and Emergency Services; the state of New York; the Research Foundation for the State University of New York (SUNY); the University at Albany, SUNY; the Atmospheric Sciences Research Center (ASRC) at SUNY Albany; and the Department of Atmospheric and Environmental Sciences (DAES) at SUNY Albany. This work could not have been done without the help of all the staff at the NYSM. Without the help of field technicians physically going to sites and witnessing freezing conditions and staff in the Operations Center noticing this pattern, this project would not have been possible. J. Wang was partially supported by the U.S. National Oceanic and Atmospheric Administration (Grant NA18OAR4310425). The ASOS data were obtained from the Iowa Environmental Mesonet (https://mesonet.agron.iastate.edu/request/download.phtml?network=NY_ASOS). The NCEI storm data were downloaded from NOAA NCEI Storm Events Database (https://www.ncdc.noaa.gov/stormevents/).

REFERENCES

Abdelaal, A., D. Nims, K. Jones, and H. Sojoudi, 2019: Prediction of ice accumulation on bridge cables during freezing rain: A theoretical modeling and experimental study. *Cold Reg. Sci. Technol.*, **164**, 102782, https://doi.org/10.1016/j.coldregions.2019.102782.

Andre, J., A. Kiremidjian, and C. T. Georgakis, 2018: Statistical modeling of time series for ice accretion detection on bridge cables. *J. Cold Reg. Eng.*, **32**, 04018004, https://doi.org/10.1061/(ASCE)CR.1943-5495.0000157.

Bragg, D. C., M. G. Shelton, and B. Zeide, 2003: Impacts and management implications of ice storms on forests in the southern United States. *For. Ecol. Manage.*, **186**, 99–123, https://doi.org/10.1016/S0378-1127(03)00230-5.

Brotzge, J., and Coauthors, 2020: A technical overview of the New York State Mesonet standard network. *J. Atmos. Oceanic Technol.*, **37**, 1827–1845, https://doi.org/10.1175/JTECH-D-19-0220.1.

Call, D. A., 2010: Changes in ice storm impacts over time: 1886–2000. *Wea. Climate Soc.*, **2**, 23–35, https://doi.org/10.1175/2009WCAS1013.1.

Changnon, S. A., 2003: Characteristics of ice storms in the United States. *J. Appl. Meteor.*, **42**, 630–639, https://doi.org/10.1175/1520-0450(2003)042<0630:COISIT>2.0.CO;2.

Cortinas, J., B. C. Bernstein, C. C. Robbins, and J. W. Strapp, 2004: An analysis of freezing rain, freezing drizzle, and ice pellets across the United States and Canada: 1976–90. *Wea. Forecasting*, **19**, 377–390, https://doi.org/10.1175/1520-0434(2004)019<0377:AAOFRF>2.0.CO;2.

Dai, A., 2008: Temperature and pressure dependence of the rain–snow phase transition over land and ocean. *Geophys. Res. Lett.*, **35**, L12802, https://doi.org/10.1029/2008GL033295.

DeGaetano, A. T., 2000: Climatic perspective and impacts of the 1998 northern New York and New England ice storm. *Bull. Amer. Meteor. Soc.*, **81**, 237–254, https://doi.org/10.1175/1520-0477(2000)081<0237:CPAIOT>2.3.CO;2.

Degelia, S. K., J. I. Christian, J. B. Basara, T. J. Mitchell, D. F. Gardner, S. E. Jackson, J. C. Ragland, and H. R. Mahan, 2016: An overview of ice storms and their impact in the United States. *Int. J. Climatol.*, **36**, 2811–2822, https://doi.org/10.1002/joc.4525.

Ding, B., K. Yang, J. Qin, L. Wang, Y. Chen, and X. He, 2014: The dependence of precipitation types on surface elevation and meteorological conditions and its parameterization. *J. Hydrol.*, **513**, 154–163, https://doi.org/10.1016/j.jhydrol.2014.03.038.

Fiebrich, C. A., 2003: Interesting ice accumulation on a cup anemometer during an Oklahoma ice storm. *Bull. Amer. Meteor. Soc.*, **84**, 551–552, https://doi.org/10.1175/1520-0477-84.5.551.

——, C. R. Morgan, A. G. McCombs, P. K. Hall Jr., and R. A. McPherson, 2010: Quality assurance procedures for mesoscale meteorological data. *J. Atmos. Oceanic Technol.*, **27**, 1565–1582, https://doi.org/10.1175/2010JTECHA1433.1.

Fikke, S. M., J. E. Kristjánsson, and B. E. K. Egil Kringlebotn Nygaard, 2008: Modern meteorology and atmospheric icing. *Atmospheric Icing of Power Networks*, M. Farzaneh, Ed., Springer, 1–29.

Homola, M. C., P. J. Nicklasson, and P. A. Sundsbø, 2006: Ice sensors for wind turbines. *Cold Reg. Sci. Technol.*, **46**, 125–131, https://doi.org/10.1016/j.coldregions.2006.06.005.

Huffman, G. J., and G. A. Norman, 1988: The supercooled warm rain process and the specification of freezing precipitation. *Mon. Wea. Rev.*, **116**, 2172–2182, https://doi.org/10.1175/1520-0493(1988)116<2172:TSWRPA>2.0.CO;2.

Irland, L. C., 2000: Ice storms and forest impacts. *Sci. Total Environ.*, **262**, 231–242, https://doi.org/10.1016/S0048-9697(00)00525-8.

Jennings, K. S., T. S. Winchell, B. Livneh, and N. P. Molotch, 2018: Spatial variation of the rain–snow temperature threshold across the Northern Hemisphere. *Nat. Commun.*, **9**, 1148, https://doi.org/10.1038/s41467-018-03629-7.

Kovacik, C., and K. Kloesel, 2014: Changes in ice storm frequency across the United States. Southern Climate Impacts Planning Program Rep., 21 pp., http://www.southernclimate.org/publications/Ice_Storm_Frequency.pdf.

Makkonen, L., P. Lehtonen, and L. Helle, 2001: Anemometry in icing conditions. *J. Atmos. Oceanic Technol.*, **18**, 1457–1469, https://doi.org/10.1175/1520-0426(2001)018<1457:AIIC>2.0.CO;2.

McCray, C. D., E. H. Atallah, and J. R. Gyakum, 2019: Long duration freezing rain events over North America: Regional climatology and thermodynamic evolution. *Wea. Forecasting*, **34**, 665–681, https://doi.org/10.1175/WAF-D-18-0154.1.

——, J. R. Gyakum, and E. H. Atallah, 2020: Regional thermodynamic characteristics distinguishing long- and short-duration freezing rain events over North America. *Wea. Forecasting*, **35**, 657–671, https://doi.org/10.1175/WAF-D-19-0179.1.

Millward, A. A., and C. E. Kraft, 2004: Physical influences of landscape on a large-extent ecological disturbance: The northeastern North American ice storm of 1998. *Landscape Ecol.*, **19**, 99–111, https://doi.org/10.1023/B:LAND.0000018369.41798.2f.

Mulherin, N. D., 1998: Atmospheric icing and communication tower failure in the United States. *Cold Reg. Sci. Technol.*, **27**, 91–104, https://doi.org/10.1016/S0165-232X(97)00025-6.

NCEI, 2019: Storm events database. NOAA, www.ncdc.noaa.gov/stormevents/.

NOAA, 1998: Automated Surface Observing System: ASOS user's guide. NOAA Doc., 74 pp.

NWS, 2016: Storm data preparation. NWS Instruction 10-1605, 110 pp., https://www.ncdc.noaa.gov/stormevents/pd01016005curr.pdf.

Rauber, R. M., L. S. Olthoff, M. K. Ramamurthy, and K. E. Kunkel, 2000: The relative importance of warm rain and melting processes in freezing precipitation events. *J. Appl. Meteor.*, **39**, 1185–1195, https://doi.org/10.1175/1520-0450(2000)039<1185:TRIOWR>2.0.CO;2.

——, ——, ——, D. Miller, and K. E. Kunkel, 2001: A synoptic weather pattern and sounding-based climatology of freezing precipitation in the United States east of the Rocky Mountains. *J. Appl. Meteor. Climatol.*, **40**, 1724–1747, https://doi.org/10.1175/1520-0450(2001)040<1724:ASWPAS>2.0.CO;2.

Reeves, H. D., 2016: The uncertainty of precipitation-type observations and its effect on the validation of forecast precipitation type. *Wea. Forecasting*, **31**, 1961–1971, https://doi.org/10.1175/WAF-D-16-0068.1.

Savadjiev, K., and M. Farzaneh, 2004: Modeling of icing and ice shedding on overhead power lines based on statistical analysis of meteorological data. *IEEE Trans. Power Delivery*, **19**, 715–721, https://doi.org/10.1109/TPWRD.2003.822527.

Sonmez, I., J. L. Schroeder, W. S. Burgett, and K. B. Haynie, 2005: The enhancement of QA/QC tests for West Texas Mesonet wind parameters. *15th Conf. on Applied Climatology*, Savannah, GA, Amer. Meteor. Soc., JP1.28, https://ams.confex.com/ams/15AppClimate/techprogram/paper_92055.htm.

Zerr, R. J., 1997: Freezing rain: An observational and theoretical study. *J. Appl. Meteor.*, **36**, 1647–1661, https://doi.org/10.1175/1520-0450(1997)036<1647:FRAOAT>2.0.CO;2.